Virologica Sinica (2020) 35:599–613
https://doi.org/10.1007/s12250-020-00226-1

www.virosin.org
www.springer.com/12250

RESEARCH ARTICLE

Myristoylation of EV71 VP4 is Essential for Infectivity and Interaction with Membrane Structure

Jiaming Cao[1] · Meng Qu[1] · Hongtao Liu[1] · Xuan Wan[1] · Fang Li[1] · Ali Hou[1,2] · Yan Zhou[1,2] · Bo Sun[1,2] · Linjun Cai[1,2] · Weiheng Su[1,2] · Chunlai Jiang[1,2]

Received: 12 December 2019 / Accepted: 3 March 2020 / Published online: 12 May 2020

Abstract

The Enterovirus 71 (EV71) VP4 is co-translationally linked to myristic acid at its amino-terminal glycine residue. However, the role of this myristoylation in the EV71 life cycle remains largely unknown. To investigate this issue, we developed a myristoylation-deficient virus and reporter (luciferase) pseudovirus with a Gly-to-Ala mutation (G2A) on EV71 VP4. When transfecting the EV71-G2A genome encoding plasmid in cells, the loss of myristoylation on VP4 did not affect the expression of viral proteins and the virus morphology, however, it did significantly influence viral infectivity. Further, in myristoylation-deficient reporter pseudovirus-infected cells, the luciferase activity and viral genome RNA decreased significantly as compared to that of wild type virus; however, cytopathic effect and viral capsid proteins were not detected in myristoylation-deficient virus-infected cells. Also, although myristoylation-deficient viral RNA and proteins were detected in the second blind passage of infection, they were much fewer in number compared to that of the wild type virus. The replication of genomic RNA and negative-strand viral RNA were both blocked in myristoylation-deficient viruses, suggesting that myristoylation affects viral genome RNA release from capsid to cytoplasm. Besides, loss of myristoylation on VP4 altered the distribution of VP4-green fluorescent protein protein, which disappeared from the membrane structure fraction. Finally, a liposome leakage assay showed that EV71 myristoylation mediates the permeability of the model membrane. Hence, the amino-terminal myristoylation of VP4 is pivotal to EV71 infection and capsid-membrane structure interaction. This study provides novel molecular mechanisms regarding EV71 infection and potential molecular targets for antiviral drug design.

Keywords Enterovirus 71 (EV71) · Myristoylation · Infectivity · Membrane structure

Introduction

Myristoylation is the covalent attachment of myristic acid, a 14-carbon saturated fatty acid, to the N-terminal glycine of proteins expressed in eukaryotic cells (Boutin 1997; Farazi *et al.* 2001; Gordon *et al.* 1991). Although often referred to as post-translational modification (PTM), myristoylation usually occurs co-translationally (Wilcox *et al.* 1987). This process is catalyzed by enzymes prevalent in eukaryotes, including N-myristoyl transferase (NMT) (Udenwobele *et al.* 2017). The binding site of myristic acid includes a consensus sequence that requires a serine (Ser) or threonine (Thr) residue in the fifth position, in addition to a Gly residue at the N-terminus ($G^1X^2X^{3-}X^4S/T^5X^6X^7X^8$) that facilitates myristoylation of many proteins (Johnson *et al.* 1994).

Electronic supplementary material The online version of this article (https://doi.org/10.1007/s12250-020-00226-1) contains supplementary material, which is available to authorized users.

✉ Weiheng Su
suweiheng@jlu.edu.cn

✉ Chunlai Jiang
jiangcl@jlu.edu.cn

[1] National Engineering Laboratory for AIDS Vaccine, School of Life Sciences, Jilin University, Changchun 130012, China

[2] Key Laboratory for Molecular Enzymology and Engineering of the Ministry of Education, School of Life Sciences, Jilin University, Changchun 130012, China

A large number of proteins with diverse functions are modified by N-myristoylation (Thinon *et al.* 2014). The prevalence of N-terminally myristoylated proteins in eukaryotes has been estimated to be between 0.5% and 3% of the cellular proteome, depending on species and the predictive model used (Martinez *et al.* 2008; Maurer-Stroh *et al.* 2002). These proteins have a broad range of functions and include protein kinases and phosphatases, G_{α} proteins, nitric oxide synthase (Braam and Verhaar 2007), ADP-ribosylation factors (ARFs), calcium-binding proteins and membrane or cytoskeleton-associated structural proteins such as MARCKS (Raju *et al.* 1995; Resh 1999). Hence, myristoylation plays an essential role in multiple cellular mechanisms.

In addition to cellular functions, myristoylated proteins are involved in a wide variety of physiological activities in viruses, including replication, assembly, and infection. For example, covalent linkage of myristic acid to an N-terminal glycine residue in Pr55gag, the precursor of major structural proteins in human immunodeficiency virus 1 (HIV-1), facilitates an essential step in virus assembly and propagation (Bryant and Ratner 1990). Myristoylation is also critical for the function of the Nef protein in HIV (Geyer and Peterlin 2001; Giese *et al.* 2006; Zhu *et al.* 2017). These studies indicate that during HIV infection, the virus anchors myristoylated Nef to the plasma membrane, where it binds to and degrades surface receptors (Hill and Skowronski 2005; Mariani and Skowronski 1993; Peng and Robert-Guroff 2001; Udenwobele *et al.* 2017). Myristoylation also occurs in murine leukemia virus (MLV) (Rein *et al.* 1986), Mason-Fisher virus (MPMV) (Rhee and Hunter 1987), and Rouse's sarcoma virus (Wills *et al.* 1989), suggesting that for any of these viruses myristoylation is a necessary step for viral infection. Moreover, the non-myristoylated spleen necrosis virus exhibits inhibition of virus replication, aberrant proteolytic processing, interruption of virion assembly, and decreased releasing of virus from cells (Weaver and Panganiban 1990). Treatment of Lassa virus-infected cells with various myristoylation inhibitors also drastically reduces efficient Lassa virus replication (Strecker *et al.* 2006), further indicating that this protein modification is crucial for viral functioning.

Myristoylation also plays a crucial role in picornaviruses. Host ribosomes translate the RNA genome of picornaviruses into a single polyprotein, precursor protein P1 (Jiang *et al.* 2014). The N-terminal glycine (position 2) of the newly formed P1 becomes rapidly modified by covalent linkage to myristic acid (Chow and Moscufo 1995; Chow *et al.* 1987; Paul *et al.* 1987). Capsid assembly begins with cleavage of P1 into VP0, VP3, and VP1 by viral protease, and assembly into protomers, which then assemble into pentamers and subsequently into an icosahedral capsid that encloses the viral RNA genome; finally, VP0, in most picornaviruses, is processed into VP4 and VP2, after which mature infectious virions are released (Mousnier *et al.* 2018). The myristic acid moiety may potentially function in the early and late processes of particle assembly (Marc *et al.* 1990; Moscufo *et al.* 1991), with two possible functions for myristoylation having been proposed during early particle assembly. First, the myristoylation of VP0 interacts with the membrane replication complex (Martin-Belmonte *et al.* 2000). Second, the myristic acid component promotes the protomer interaction of the pentameric assembly (Ansardi *et al.* 1992; Lee and Chow 1992), similar to functions proposed for myristoylation during the pentamer formation of foot-and-mouth disease virus capsid (Goodwin *et al.* 2009). VP0 myristoylation also appears to be important in the later period of poliovirus (PV) assembly during virus maturation (Ansardi *et al.* 1992; Marc *et al.* 1990; Moscufo *et al.* 1991).

Enterovirus 71 (EV71) is a member of *Picornaviridae* family and is an important pathogen in hand, foot, and mouth disease. Further, neurological complications may develop with the potential to inflict permanent morbidity or even fatality, thereby posing significant public health concerns, specifically for infants and children (Alexander *et al.* 1994; Chumakov *et al.* 1979; Lum *et al.* 1998). The EV71 VP4 is also co-translationally linked to myristic acid at its amino-terminal glycine residue (position 2) (Chow *et al.* 1987); however, the role of myristoylation in EV71 remains largely unknown.

In this study, we constructed myristoylation-deficient EV71 models with Gly-to-Ala mutation (G2A), and analyzed viral genome RNA replication and assembly in both the reporter pseudovirus system and live virus system. Using these virus models, we found that loss of myristoylation had a severe effect on viral infectivity. Furthermore, we examined the interaction between myristyl groups and membrane structure, as well as the possible mechanism of myristoylation in the EV71 virus.

Materials and Methods

Cells

The SV40-transfected human embryonic kidney 293 cell line HEK293T was cultured as a monolayer in Dulbecco's Modified Eagle medium (DMEM) supplemented with 10% fetal calf serum (FCS). HEK293S cells stably expressing SCARB2 (Li *et al.* 2013), which is the EV71 receptor, were cultured as monolayers in DMEM supplemented with 10% FCS and 1.25% puromycin as selective media for SCARB2 expression.

Plasmid Construction and Virus Production via Reverse Genetics Approach

Production of Wild Type (WT) or G2A Reporter Pseudoviruses

We employed the previously published plasmid, GFP-P1-WT (Jin *et al.* 2012), composed of green fluorescent protein (GFP) and EV71 *P1* genes with a linker coding the EV71 $2A^{pro}$ cleavage motif (KGLTTY↓G, where the arrow indicates the cleavage site). To abolish the myristoylation signal, we generated a G2A mutation by site-directed mutagenesis of the codon specifying the second amino acid of P1, a glycine (which is also the second amino acid of VP4) (Krausslich *et al.* 1990). P1 of the EV71 introduced a glycine to alanine (G2A) mutation using primers 5′-CTAAACATGGCTTCGCAAGTG-3′ and 5′-CACTTGCGAAGCCATGTTTAG-3′, and the mutant sequence was confirmed by sequence analysis by Comate Bioscience Company Limited. The plasmids, pcDNA3.1-T7 RNA Pol and pBS-T7-EV71-luciferase, were constructed as described previously (Jin *et al.* 2013). T7 RNA polymerase expression plasmid (pT7 RNA Pol), was used for expressing T7 RNA polymerase. The pT7-EV71-luciferase replicon plasmid is a reversely transcribed full-length EV71 genome encoding the firefly luciferase gene in place of the *P1* gene, which can be packaged in the nuclei of virus particles; and EV71 capsid expression plasmid (pGFP-P1-WT or pGFP-2A-P1-G2A), which expresses the EV71 capsid proteins as a fusion protein with GFP under the control of the cytomegalovirus (CMV) promoter, and can trans-encapsidate the full-length EV71 genome (Jin *et al.* 2012).

EV71 reporter pseudoviruses were produced following cotransfection of 293T cells with three plasmids pGFP-P1-WT or pGFP-2A-P1-G2A, pT7-RNA-pol and pT7-EV71-luciferase (Arita *et al.* 2006; Jin *et al.* 2013; Xu *et al.* 2014). Briefly, in a 6 wells plate, a 70% confluent monolayer of 293T cells was co-transfected with 1 μg of each of pT7-RNA-pol, pT7-EV71-luciferase and pGFP-2A-P1 or pGFP-2A-P1-G2A in 10 μL of Lipofectamine2000 reagent (Invitrogen, California, USA) and incubated at 37 °C in 1 mL DMEM (Jin *et al.* 2012). The cells were washed, and 10% FCS-DMEM was added to the cells at 6 h post-transfection and then incubated for 48 h. The supernatant (containing the virions) from cell cultures was then harvested and stored at − 80 °C.

Production of WT or G2A Live Virus

The plasmid pwsk-T7-EV71 (WT) containing full-length EV71 genome (C4b) was constructed as described previously (Cao *et al.* 2019). To generate the G2A mutation, a similar protocol as that described for G2A reporter luciferase pseudoviruses was followed. This was facilitated by cloning the 5′-terminal sequences of EV71 into a vector suitable for mutagenesis. The *Sph*I-*Bam*HI DNA fragment (nucleotides [nt] 1751–2667) of pwsk-T7-EV71 was inserted into the polylinker region of plasmid VR1012 (Invitrogen, USA). The primers used for the mutation were the same as those used to mutate the G2A reporter luciferase pseudoviruses at the second amino acid of P1 (glycine to alanine, G2A). The mutant sequence was confirmed by sequence analysis. The mutant *Sph*I-*Bam*HI fragment of VR1012 (corresponding to nt 1751–2667 of the pwsk-T7-EV71) was cloned back into the *Bam*HI-*Sph*I fragment of plasmid pwsk-T7-EV71, and the mutations were verified by sequence analysis.

EV71 live viruses were produced through cotransfecting 293T cells with pT7-EV71-WT or pT7-EV71-G2A, and pT7-RNA-pol (Cao *et al.* 2019). Briefly, in a 6 wells plate, a 70% confluent monolayer of 293T cells was co-transfected with 1 μg pT7-RNA-pol and pT7-EV71-WT or pT7-EV71-G2A in 6 μL of lipofectamine2000 reagent (Invitrogen) and incubated at 37 °C in 1 mL of DMEM. The cells were washed, and 10% FCS-DMEM was added to the cells at 6 h post-transfection and incubated for 48 h. The supernatant of cells was then harvested and stored at − 80 °C.

VP4-WT-GFP or VP4-G2A-GFP Expression Plasmid

To observe the intracellular distribution of proteins with or without myristoylation, we constructed the plasmid VP4-WT-GFP and VP4-G2A-GFP, which was composed of VP4-WT or VP4-G2A genes and GFP. Briefly, the VP4-G2A gene was synthesized by PCR with the template for the pGFP-2A-P1-G2A plasmid, and the template for VP4-WT genes was pGFP-2A-P1. At the 5′ end of the VP4 sequence, we created the *Not*I restriction sites by PCR, while at the 3′ end we synthesized 20 nucleotides, which were the same as the 5′ end of GFP gene. The GFP gene was also synthesized by PCR with the template of the pGFP plasmid. At the 3′ end of the GFP sequence, we created the XbaI restriction sites by PCR. Vector VR1012 cleaved at the *Not*I, and *Xba*I site and three fragments: VP4-WT or VP4-G2A, GFP, and *Not*I-*Xba*I fragment were isolated in a low gelling temperature agarose gel. The VP4-WT or VP4-G2A and GFP fragments were mixed for homologous recombination as instructed with In-Fusion® HD Cloning Kit (Takara) user manufacture. Then the VP4-WT-GFP or VP4-G2A-GFP fragment was inserted into the NotI-XbaI fragment of plasmid VR1012 and plasmid pVP4-WT-GFP or pVP4-G2A-GFP was verified by sequence analysis.

Peptide Synthesis

The WT-VP4 or G2A-VP4 full-length peptides, the WT-VP4 or G2A-VP4 short peptides including the first 20 amino acids of VP4 (EV71-WT or G2A-VP4-20aa), and HRV VP4 confirmed to induce permeability in model membranes (Zauner *et al.* 1995) were obtained from GL Biochem (Shanghai, China). The sequences of the polypeptides are shown in Table S1.

The purity of the peptides was determined by analytical reverse-phase high-pressure liquid chromatography (RP-HPLC) using a C18 column, and peptide masses were confirmed by time-of-flight mass spectrometry performed with an LTQ Orbitrap Velos mass spectrometer (Thermo, CA, USA). Purified peptides were stored at − 80 °C (Zauner *et al.* 1995). The data is presented in Supplementary Fig. S1.

Western Blotting

Whole-cell extracts were prepared by cell lysis in RIPA buffer for 30 min on ice and clarified at 20,000 ×*g* for 5 min at 4 °C. The supernatants were added to SDS-PAGE sample buffer, boiled, and separated in 13.5% polyacrylamide gels. Proteins were electro-transferred onto PVDF membranes for Western blot analysis. Membranes were probed with rabbit anti-VP3, anti-VP2, and anti-VP1 polyclonal antibodies (1:1000, GeneTex, USA) in PBS with 1% skim milk, followed by probing with a corresponding alkaline phosphatase (AP)-conjugated secondary antibody (Sigma, St. Louis, MO, USA) that was diluted 1:10,000. And the immunoreactions were visualized with nitro blue tetrazolium (NBT, Dinguo, Beijing, China) and 5-bromo-4-chloro-3indolyl phosphate (BCIP, Dinguo) solutions.

Transmission Electron Microscopy

To perform transmission electron microscopy (TEM), WT or G2A reporter pseudoviruses were obtained from transfected 293T cells. Briefly, after two rounds of freezing and thawing, the transfected 293T cell lysates were filtered through a 0.22-μm membrane. WT or G2A reporter pseudoviruses were purified from the resulting suspension using DEAE-Sepharose (Amersham Pharmacia Biotech, Piscataway, NJ, USA) (Horodniceanu *et al.* 1979), followed by centrifugation at 100,000 ×*g* for 2.5 h at 4 °C in a Beckman SW40 rotor through a 1 mL 30% sucrose cushion. The pellet was washed thrice with distilled water and dissolved in 500 μL phosphate-buffered saline (PBS). Samples were examined by TEM (JEM-1220; JEOL Datum, Tokyo, Japan) at an acceleration voltage of 80 kV, and the images were obtained at 200,000× magnification (Jin *et al.* 2013).

High-Pressure Cryo-electron Microscope

HEK293T cells were co-transfected with pT7 RNA Pol (Xu *et al.* 2014) and pT7-EV71-WT or G2A using lipofectamine 2000 follow the instructions provided by the manufacturer (Invitrogen, Carlsbad, CA, USA). After 48 h, the cells were collected with 1 × PBS and centrifuged at 300 ×*g* for 5 min, after which the supernatant was discarded. Next, 1 mL acetaldehyde fixing solution was added to precipitate the cells into a spherical shape. The samples were sent to the China National Biological Products Institute, and the high-pressure frozen tablets were then observed by transmission electron microscopy.

Luciferase Reporter Gene Assay

Reporter pseudoviruses were collected from the supernatants, which were serially diluted fivefold in DMEM (10% FCS) and used to inoculate 293S cells (4×10^4 cells per well) in quadruplicate in 96-well plates (BD Biosciences). These cultures were incubated for 18 h at 37 °C, after which the cells were harvested for luciferase activity measurement using a luciferase assay kit (Promega, USA) according to the manufacturer's recommendations. Briefly, cells were lysed in 100 μL reporter lysis buffer (Promega, USA), and luciferase activity in cell lysates (100 μL per well) was measured using a VICTOR^{TM} × 2 Multilabel Plate Reader (Perkin Elmer, UK).

Cytopathic Effect Assay (CPE)

293S cells were added to the plates at 90% confluency. A virus with the equal amount of viral RNA load was used to inoculate individual wells of the 6-well plates. The plates were incubated at 37 °C with 5% CO_2 for 1 h, with agitation every 15 min. The virus inoculums were then discarded; cells were washed thrice with 1 × PBS and inoculated with 2 mL DMEM medium containing 10% FCS. The cells were observed daily.

Infected Cells Blind Passage

In a 12-well plate, a 70% confluent monolayer of 293S cells was infected with live-WT and G2A viruses with an equal amount of RNA. At 1 h post-infection, the virus supernatant was discarded, fresh medium was added and incubated for 24 h. These cells were denoted as the P0 generation cells (P0) and were resuspended, added to a fresh 6-well plate with fresh medium added to allow for cell proliferation. After 24 h, the cells covering the 6-well

plates were denoted the P1 generation cells (P1), which were then placed in a fresh T25 flask with fresh medium to continue the culture. After 24 h at 37 °C, the cells that covered with the T25 flask were designated the P2 generation (P2). Half of the P0 and P1 cells were used to measure the amount of viral RNA, while the other half was used for cell passaging. Half of the P2 cells were used for measuring viral RNA and the other half were added to a new well in a 6-well plate and used for immunofluorescence assaying once the cells had attached.

Viruses Infected Cells with Inhibitor

Live WT viruses with equal amount viral RNA infected 293S cells treated with a final concentration of 100 μmol/L 2-HMA or without 2-HMA. After cells without 2-HMA produced CPE, Progeny non-myristoylated viruses were then collected from cells with 2-HMA, and used in infection for construction of a growth curve. WT, G2A live virus and Progeny non-myristoylated viruses containing an equal amount of viral RNA infected 293S cells. NH_4Cl at a final concentration of 40 mmol/L was used to treat 293S cells 2 h before infection with live WT virus, and after infection. Negative viral RNA content was then measured.

Quantitative Reverse Transcription-Polymerase Chain Reaction (qRT-PCR)

The total RNA of cells infected with WT or G2A virus or reporter pseudovirus was extracted using the RNAprep pure CellorBacteria kit (TIANGEN Biotech Co., Ltd, Beijing, China) according to manufacturer's instructions. cDNA was synthesized using the Prime Script™ RT reagent kit with gDNA Eraser (Takara, Japan), and cDNA levels were quantified using real-time PCR (SYBR Green™ *Premix Ex Taq*™, Takara, Japan) using primers EV71-5′UTR-F (5′-TCCTCCGGCCCCTGA-3′) and EV71-5′UTR-R (5′-AATTGTCACCATAAGCAGCCA-3′) targeting the EV71 5′ UTR. The *GAPDH* gene was used as an internal control to normalize the total RNA in the samples.

Immunofluorescence Assay

293S cells infected with WT and G2A live virus were fixed with 4% paraformaldehyde for 15 min and treated with 0.2% Triton X-100 for 15 min, blocked with 1% bovine serum albumin for 1 h, and subsequently incubated with an anti-EV71 VP3 rabbit polyclonal antibody prepared as previously reported (Zhang *et al.* 2012) for 2 h, followed by reaction with a FITC-goat anti-rabbit antibody (Bioss Biotech Co., Ltd, Beijing, China) for 1 h. The cell nuclei were stained with DAPI (Key GEN Biotech Co., Ltd, Nanjing, China). Fluorescence was recorded using the Zeiss LSM 710 (Zeiss, Jena, Germany).

Quantification of Negative-Strand Genomic RNA

The release of viral mRNA into the cytoplasm is a prerequisite for enabling replication of viral RNA to allow for replication of the viral negative-strand RNAs. Hence, the amount of negative-strand RNA is reflective of whether viral mRNA is released into the cells (Zhang *et al.* 2017). Quantification of negative-strand genomic RNA replication was performed as previously described (Zhang *et al.* 2017), and the total RNAs of the infected cell samples were extracted and subjected to RT-PCR quantification as described previously (2.10). In brief, cDNA was synthesized with a Prime Script™ RT reagent kit with gDNA Eraser (Takara, Japan) using a primer specific to the negative-strand genomic RNA (1F: 5′-TTAAAACAGCCTGTGGGTTG-3′) (Zhang *et al.* 2017). The cDNA synthesized from negative-strand genomic RNA was then quantified with real-time PCR using 5′ UTR specific primers. The *GAPDH* gene was used as an internal control to normalize the total RNA of the sample.

Confocal Microscopy

293T cells were grown until subconfluency in 24-well plates was achieved. Cells were transfected with pVP4-WT-GFP or pVP4-G2A-GFP and incubated for 24 h, after which the cells were washed with PBS, fixed with 4% paraformaldehyde, and permeabilized with PBS containing 0.5% saponin. Samples were blocked for 15 min in 0.5% fish gelatin in PBS. Cell nuclei were counterstained with DAPI. All steps were carried out at room temperature. The samples were examined with an LSM 700 confocal laser scanning microscope (Zeiss), and images were processed with ImageJ.

Cytoplasmic and Membrane Fractionations

Cytoplasmic and membrane fractionations were examined as previously described (Colomer-Lluch and Serra-Moreno 2017). Briefly, 5×10^6 293T cells were transfected with 5 μg pVP4-WT-GFP or pVP4-G2A-GFP plasmid for 24 h. Cells were then lysed, and sequential extraction of proteins from specific cellular compartments and/or organelles was performed using the ProteoExtract® Subcellular Proteome Extraction kit (S-PEK, Millipore, Bedford, MA USA) following the manufacturer's instructions. Cytoplasmic fraction (F1) and membrane protein fraction (F2) were analyzed via western blotting using an anti-GFP monoclonal antibody. Whole-cell extracts were confirmed by blotting for total protein. The membrane and cytoplasmic

fractions were determined by detecting GAPDH (cytoplasmic marker).

Liposome Leakage Assay

The ability of the compounds to disrupt model lipid membranes was assayed by the release of a fluorescent dye from liposomes loaded with a self-quenching concentration of carboxyfluorescein (Wagner *et al.* 1992). To verify the membrane interaction of myristoylation, a liposome leakage assay was performed as described previously (Zauner *et al.* 1995). Briefly, liposomes were prepared from egg phosphatidylcholine (Avanti Polar Lipids) by reverse-phase evaporation with an aqueous phase of 100 mmol/L carboxyfluorescein (CF)-50 mmol/L NaCl and extruded through a 100-nm polycarbonate filter to obtain a uniform size distribution. The liposomes were separated from unincorporated material by gel filtration through Sephadex G-25 with an iso-osmotic buffer (200 mmol/L NaCl, 25 mmol/L HEPES pH 7.3). Next, 80 μL of liposome solution was added to 80 μL peptide for a final concentration of 30 nmol/L in water in a 96-well microtiter plate (final lipid concentration, 25 μmol/L) and assayed for CF (Carboxyfluorescein) fluorescence at 485–520 nm on a VICTOR^{TM} × 2 Multilabel Plate Reader (Perkin Elmer, UK). The test time was 30 min, during which the fluorescence value was recorded every minute.

Statistical Analysis

All experiments were repeated thrice independently. The values were expressed as the mean ± standard deviation (SD). Statistical analysis was performed using a one-way ANOVA to compare the differences in test values between the experimental and control groups. Statistical significance represented by asterisks was marked correspondingly in the figures, where $*P < 0.05$, $**P < 0.01$, $***P < 0.001$, *ns*: non-significant.

Results

Protein Expression and Virus Morphology are Normal in G2A Virus and G2A Reporter Pseudovirus

In the myristoylation-deficient (G2A) reporter pseudovirus system, an equal amount of pGFP-2A-P1-WT or pGFP-2A-P1-G2A, pT7-EV71-luciferase and pT7-RNA-Pol were co-transfected into HEK 293T cells to encapsidate reporter pseudovirus. After 48 h post transfection, the cells containing reporter pseudovirus were lysed for detection of viral protein expression by Western blotting; while the supernatant was collected from the cell culture and concentrated 150-fold for detection of encapsidated virions by Western blotting and observation of virus morphology by TEM. As shown in Fig. 1A, 1B. The viral VP3 protein, a capsid protein of EV71, was detected in the G2A virus group, indicating that G2A protein expression was normal. Furthermore, TEM analyses revealed G2A virus particles were nearly 30 nm in diameter, which was consistent with the shape and size of WT EV71.

In myristoylation-deficient (G2A) virus system, an equal amount of pT7-EV71-WT or pT7-EV71-G2A and pT7-RNA-Pol were co-transfected into HEK 293T cells to encapsidate virus. The supernatants were concentrated 150-fold and used for Western blotting, while the cell lysates were collected for high-pressure cryo-electron microscopy. As shown in Fig. 1C, 1D. The results of Western blot analysis indicated that the viral VP3 protein was expressed in the G2A virus group, indicating that protein expression of G2A virus was normal. Furthermore, Cryo-SEM analyses revealed G2A virus particles were almost 30 nm in diameter and consistent in shape and size compared with WT EV71. From these experimental results, we show that in either virus system, the loss of myristoylation does not affect the normal expression of viral proteins or the morphology of the viral particles.

G2A Mutation Causes Reduce of Viral Infectivity

The loss of myristoylation did not affect virus synthesis via plasmid transfection; however, whether it affects the virus in other aspects remained unclear. To further explore the role of myristoylation in EV71, we used the G2A reporter pseudovirus and live virus to infect cells. In the reporter pseudovirus system, WT and G2A reporter pseudovirus, with equal amounts of viral RNA, were used to infect 293S cells (293T cells with stable expression of EV71 receptor SCARB2), and infectivity was determined by measuring luciferase activity. An approximately 18 h post-infection (hpi), the infected cells were collected, and the level of intracellular fluorescent expression was measured. As shown in Fig. 2A, we found that the fluorescent activity decreased to 1/500 in the G2A reporter pseudovirus compared with the pseudo-WT after infection. We subsequently measured the amount of intracellular viral RNA 24 h after infection and compared it with that of pseudo-WT. Results showed that the amount of intracellular viral RNA extracted from cells infected with G2A reporter pseudovirus decreased to 1/50 comparing to the pseudo-WT (Fig. 2B). We also sought to compare the infectivity of pseudo-WT and pseudo-G2A in 293T cells. However, this proved difficult as 293T cells were resistant to infection by both pseudoviruses (Supplementary Fig. S2).

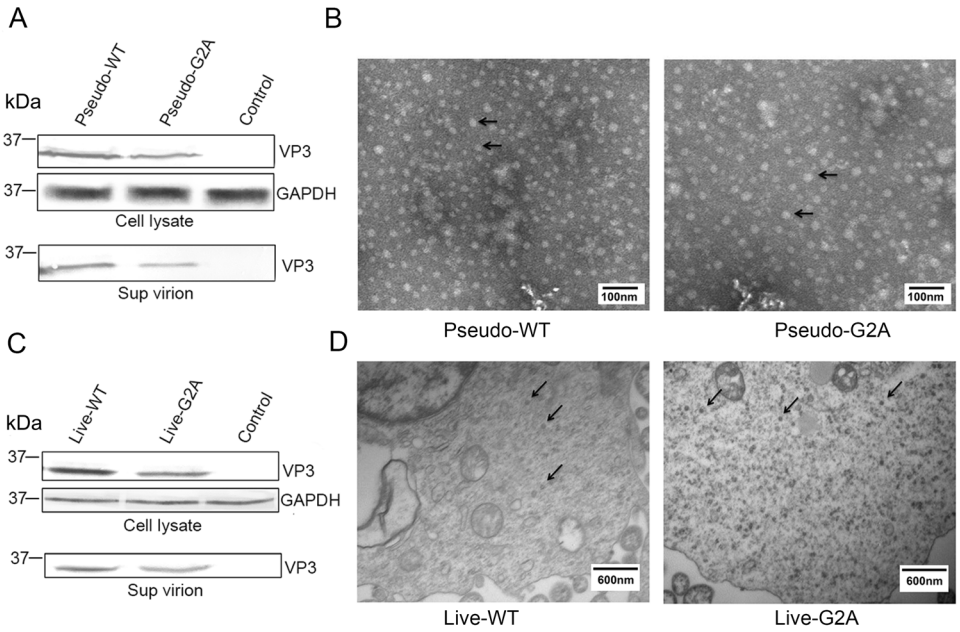

Fig. 1 Effect of myristoylation on viral protein expression and morphology of virus particles. **A** Western blotting analysis of the cell lysate and supernatant of cells transfected with pGFP-2A-P1-WT or pGFP-2A-P1-G2A using rabbit anti-VP3 poly antibody. Sup virion: virions in supernatant. Pseudo-WT: wild type pseudovirus; Pseudo-G2A: myristoylation-deficient pseudoviruses; Control: supernatant of 293T cells transfected with empty vector. GAPDH: internal control. **B** Transmission electron microscope images of myristoylation and myristoylation-deficient (G2A) reporter pseudoviruses. The arrow points to the virus particles. Scale bar, 100 nm. **C** Western blotting analysis of the cell lysate and supernatant of cells transfected with pT7-EV71-WT or pT7-EV71-G2A using rabbit anti-VP3 poly antibody. Sup virion: virions in supernatant. Live-WT WT: live myristoylation virus; Live-G2A: live myristoylation-deficient viruses. Control: supernatant of 293T cells transfected with an empty vector. GAPDH: internal control. **D** High-pressure cryo-electron microscopy images of myristoylation and myristoylation-deficient (G2A) viruses. The arrow points to the virus particles. Scale bar, 600 nm.

In the myristoylation-deficient (G2A) virus system, WT and G2A live viruses with equal amounts of viral RNA were used to infect 293S cells, and 1 h post-infection, the virus supernatant was discarded and fresh medium was added to the cell culture. Cells were continuously observed and CPE development was noted. As shown in Fig. 2C, the results showed that over time, the live-WT virus group developed cytopathic effects, while no cytopathic effect was observed in the live-G2A virus treatment group. The cells were then harvested for Western blotting analysis, results from which showed that no viral proteins were detected in the live-G2A group compared to the live-WT (Fig. 2D). Based on these results, we speculated that CPE and viral proteins were not detectable in the live-G2A group due to the low infectivity of this virus.

We next performed blind passages of cells infected with WT or G2A live virus, carrying equal amounts of viral RNA, to generate virus accumulation for subsequent detection (Fig. 2E). After 24 h infection (P0), living 293S cells were transferred to new larger culture plates. As the cell culture area expanded, the cells proliferated (P1), meanwhile viruses were permitted to undergo continuous replication. Similar passaging was repeated with a 24 h interval to reach P2 cells. Since high MOI of EV71 virus could cause rapid CPE, we reduced the initial feeder virus concentration used to infect 293S cells to maintain live cells throughout the blind passages. As shown in Fig. 2E, the amount of live-WT viral RNA increased rapidly over time. Although the amount of live-G2A viral RNA also increased, it was significantly lower than that observed for the WT group. Furthermore, immunofluorescence analysis of EV71 VP3 protein level in P2 cells (Fig. 2F) revealed both live-WT and live-G2A viral proteins were observed in cells. The difference was that viral protein expression in live-WT infected cells was pervasive and strong, whereas it was sporadic and weak in live-G2A infected cells. From these results we determined that loss of myristoylation affected viral infection, and impacted viral RNA replication specifically, thereby causing reduced viral infectivity.

Viral Genomic RNA Replication is Blocked in Cells Infected with G2A Viruses

To determine the cause for the reduced viral RNA replication in G2A live virus, we measured the growth curve of the WT and G2A live viruses over 48 h. WT and G2A viruses carrying an equal amount of viral RNA were used to infect 293S cells, which were then harvested at different time points post-infection to measure the amount of viral RNA produced in the cells. As shown in Fig. 3A, we found

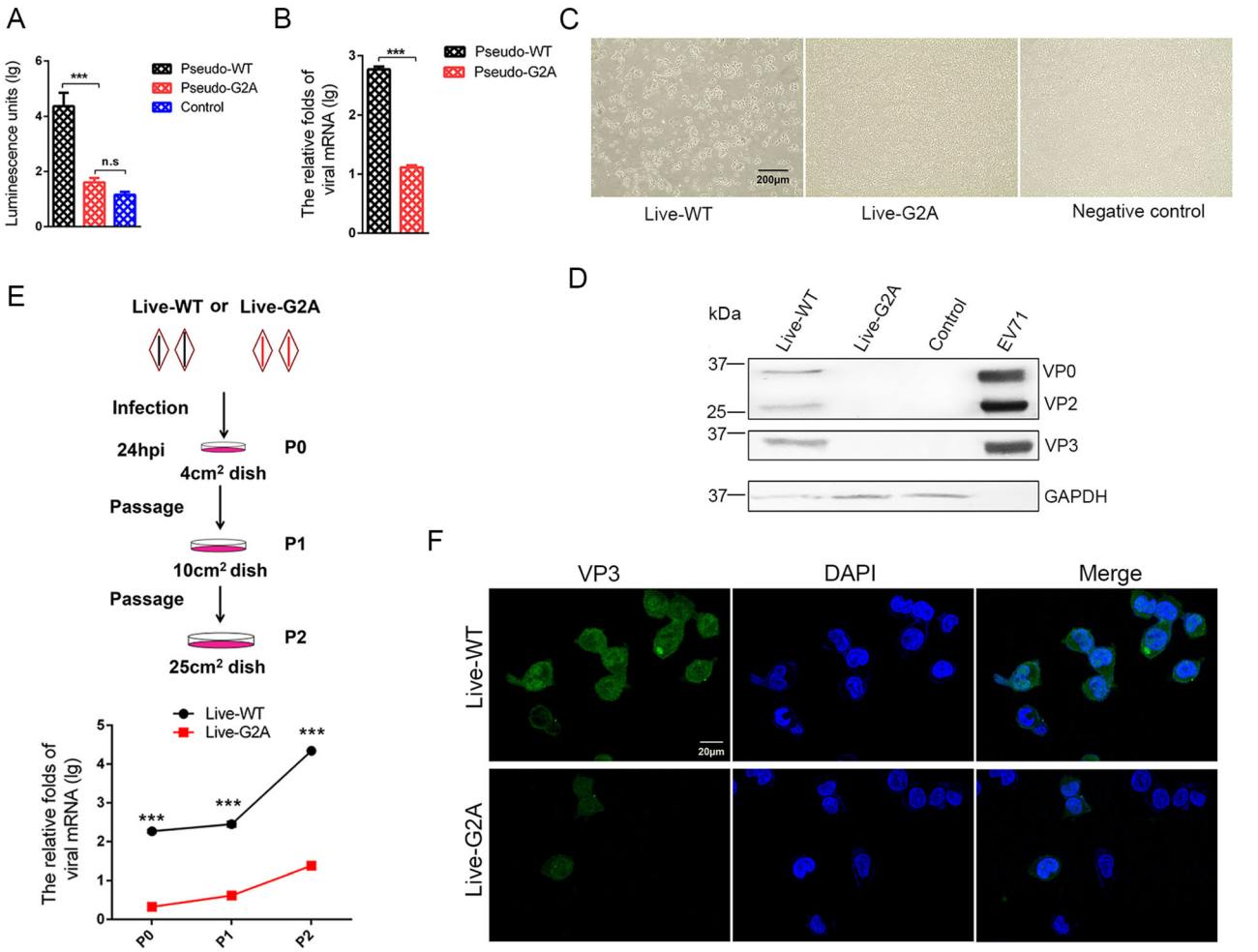

Fig. 2 Effect of myristoylation on virus infectivity. **A** Luciferase activity analysis, **B** RNA content analysis of myristoylation-deficient (G2A) reporter pseudovirus compared to the Pseudo-WT virus. Myristoylation and myristoylation-deficient (G2A) reporter pseudoviruses with the equal amount viral RNA infected 293S cells, luciferase activity and viral RNA amount were detected 18 h and 24 h respectively after infection. Control represents empty cells that were not infected. Data presented as mean ± SD of three independent experiments. $***P < 0.001$. *ns* non-significant. **C** Representative photography of cytopathic effects (CPE) analysis of myristoylation-deficient (G2A) virus compared to the WT virus. Myristoylation and myristoylation-deficient (G2A) viruses with the equal amount viral RNA infected 293S cells. At 72 hpi, the cells produced cytopathic effects (CPE) and were photographed and recorded. Live-WT: live myristoylation virus; Live-G2A: live myristoylation-deficient viruses. Scale bar = 200 μm. **D** Western blot analysis of cells infected with myristoylation-deficient (G2A) virus indicates altered protein expression compared to the WT virus with anti-EV71 VP2/VP3 rabbit polyclonal antibody. GAPDH was the internal control. EV71 inactivated virus was a positive control and 293S was the empty cell control. **E** The scheme of infected cell blind passages and the measurement of viral RNA in each passage. Myristoylation (WT) and myristoylation-deficient (G2A) viruses with an equal amount of viral RNA infected 293S cells are denoted as P0. After 24 hpi, the cells were passaged twice blindly at a 24 h interval, denoted as P1 and P2. In each passage, living cells were resuspended and transferred to a new, larger dish. Half of the cells in each passage were lysed for intracellular viral RNA extraction and quantification via qRT-PCR. The mRNA levels of viruses were normalized to GAPDH mRNA. Live-WT: live myristoylation virus; Live-G2A: live myristoylation-deficient viruses. $***P < 0.001$. **F** Confocal microscopy images of P2 generation cells infected with WT and G2A virus. WT and G2A live virus were incubated with an anti-EV71 VP3 rabbit polyclonal antibody stained green, and the nuclei were stained blue. Scale bar = 20 μm.

that the amount of live-WT viral RNA was significantly higher than that of live-G2A. To support our results, in addition to mutating the site of myristoylation, we also employed the myristic acid inhibitor, 2-Hydroxymyristic acid (2-HMA, Sigma, USA) which competitively blocks covalent attachment of myristic acid to the peptide chain (Corbic Ramljak *et al.* 2018; Tan *et al.* 2016) as a positive control for myristoylation inhibition. The 293S cells contained a final concentration of 100 μmol/L 2-HMA and were infected with the live-WT virus. Progeny non-myristoylated viruses were then collected and used in infection for measurement of growth curves. The single growth curves of the live-WT, live-G2A virus, and 2-HMA treated live-WT virus were measured at indicated time

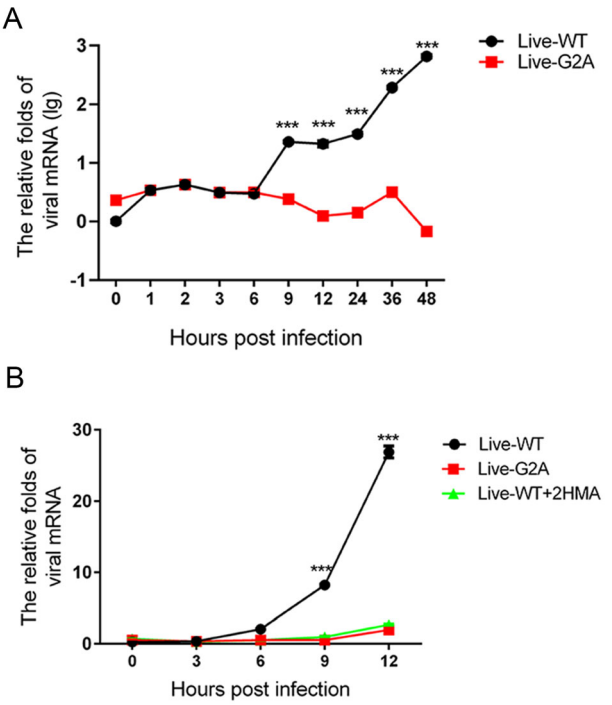

Fig. 3 Effect of myristoylation on virus RNA replication. **A** The growth curve of myristoylation and live G2A viruses. Live WT and G2A viruses containing an equal amount of viral RNA infected 293S cells. Cells were harvested 0, 1, 2, 3, 6, 9, 12, 24, 36, 48 hpi. Cellular RNA was extracted and quantified with real-time PCR. The mRNA levels of viruses were normalized to GAPDH. $***P < 0.001$. **B** The growth curve of WT, G2A live virus, and progeny non-myristoylated viruses. Cells were harvested at indicated times; viral RNA was extracted and quantified with real-time PCR. The mRNA levels of viruses were normalized to GAPDH. Data presented as mean ± SD of three independent experiments. Live-WT: live myristoylation virus; Live-G2A: live myristoylation-deficient viruses. Live-WT + 2 HMA: Progeny non-myristoylated viruses; $***P < 0.001$.

points. As shown in Fig. 3B, we found that the rate of virus replication among the three groups did not differ significantly at 3 hpi. However, from 6 hpi, the replication rate of live-WT increased rapidly; while, the viral RNA of live-G2A and 2-HMA-treated live-WT groups increased by only 1.96 and 2.69 times, respectively, at 12 hpi. These results suggest that loss of myristoylation blocks efficient virus replication.

Myristyl Group Affects Early Steps in Viral Infection

In addition, compared to the total RNA, the amount of negative-stranded RNA was also measured since during EV71 viral RNA replication, the virus must synthesize negative-stranded RNA using virus mRNA as a template (Paul *et al.* 2000). To this end, live-WT and G2A viruses carrying an equal amount of viral RNA were used to infect 293S cells with or without 2-HMA. In addition to 2-HMA, we also used another inhibitor, NH_4Cl. EV71 viruses enter their host cells by receptor-mediated endocytosis accompanied by destabilization of the endosomal membrane and release of viral genome into the cytoplasm (Lin *et al.* 2012). Specific compounds, such as NH_4Cl (Eash *et al.* 2004; Olokoltsov *et al.* 2007), are capable of inhibiting endocytosis. Hence, we chose to include such an inhibitor to verify whether this phenomenon is consequential for EV71 RNA release. We added 40 mmol/L NH_4Cl to cells before EV71 infection. As described previously, WT and G2A viruses carrying an equal amount of viral RNA were used to infect 293S cells with or without the two inhibitors, after which we measured the amount of viral negative RNA at different time points. As shown in Fig. 4. We found that the amount of negative RNA for the WT virus increased over time, while that of G2A viruses remained unchanged. Hence, the loss of myristoylation on VP4 appeared to block the generation of negative RNA, with the same result observed in virus-infected cells with inhibitors. According to these results, we conclude that viral RNA was prevented from being released into the cells infected with G2A viruses. The decrease of viral mRNA releasing is seemingly related to the early events of viral infection. Conversely, loss of myristoylation does not affect virus binding to entry into the host. Since the capsid VP4 protein linked to the myristoylation was on the interior of the capsid (Chow *et al.* 1987; Filman *et al.* 1989), it would not be capable of directly contacting the host cell surface.

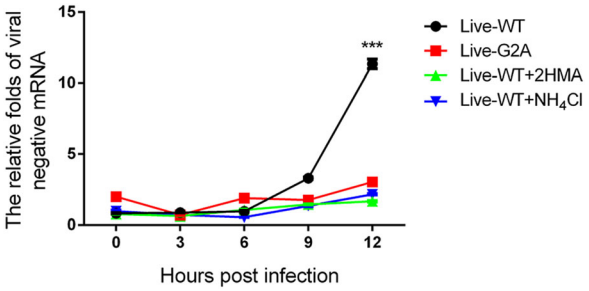

Fig. 4 Negative viral RNA content in cells with or without inhibitors infected with WT and G2A live viruses. 293S cells without NH_4Cl were infected with live WT, G2A virus and progeny non-myristoylated viruses, and cells with NH_4Cl were infected with live WT virus. Cells with or without NH_4Cl were harvested at indicated time points. Negative viral RNA content was then measured. The RNA levels of viruses were normalized to GAPDH. Data presented as mean ± SD of three independent experiments. Live-WT: live myristoylation virus; Live-G2A: live myristoylation-deficient viruses. Live-WT + 2 HMA: Progeny viruses without myristoylation, Live-WT + NH_4Cl: live myristoylation virus infected cells with inhibitor NH_4Cl, $***P < 0.001$.

The Myristyl Groups Interact with the Host Cell Membrane Structure

It has been clearly reported that myristic acid generally interacts with membrane structures (Wright *et al.* 2010) as that has been demonstrated in various viruses (Strecker *et al.* 2006; Wright *et al.* 2010; Zhu *et al.* 2017). Hence, we suggested that myristyl groups may also interact with the cell membrane for EV71. To this end, pVP4-WT-GFP or pVP4-G2A-GFP were transfected into 293T cells, protein localization was observed using laser scanning confocal microscopy after 24 h. We found that the localization of VP4-G2A-GFP changed significantly compared to the WT (Fig. 5A). The distribution of WT VP4 proteins followed normal aggregation patterns; while the distribution of proteins in G2A mutants was diffuse throughout the cytoplasm. A certain amount of VP4-G2A-GFP and VP4-WT-GFP proteins were also observed in the nucleus, however, a smaller amount was found in the latter compared to the former. Plasmid-transfected cells were harvested and the cytoplasm and membrane structures were separated for Western blot analysis and determination of VP4 protein proportion in the cytoplasm or membrane based on band grayscale in Western blot. As shown in Fig. 5B, C, 71.6% of VP4-WT-GFP proteins were distributed in membrane structures and 25.9% was distributed in cytoplasm. Conversely, only 19.2% of VP4-G2A-GFP proteins were distributed in the membrane structures, while 66.4% were distributed throughout the cytoplasm. From these results, we determine that myristyl groups interact with host membrane structures.

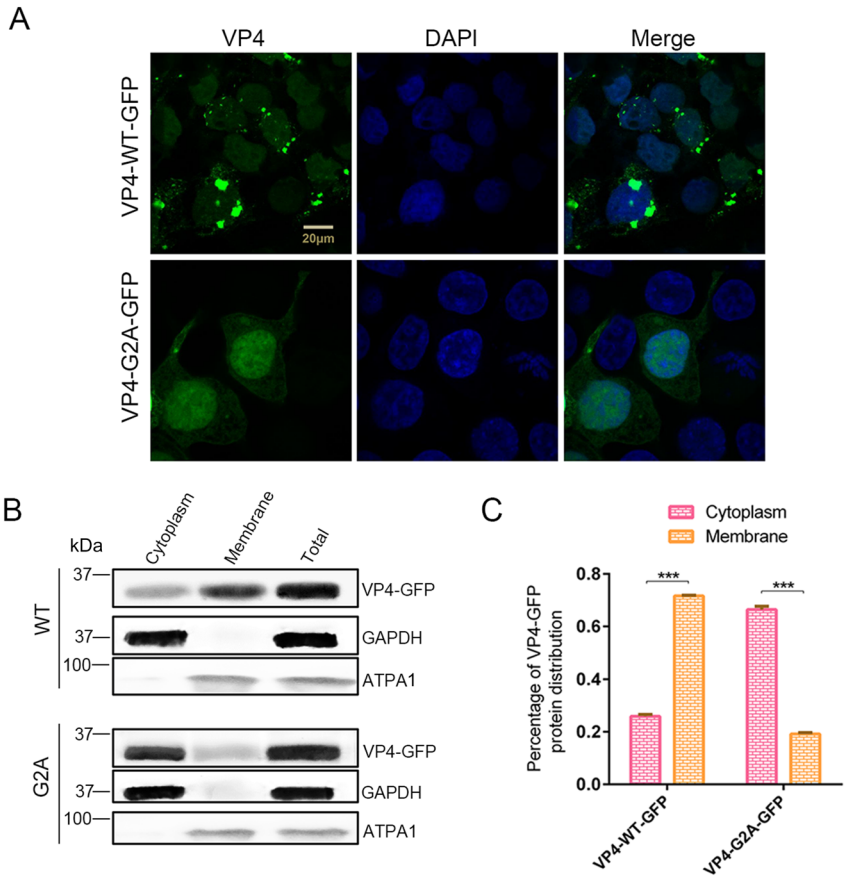

Fig. 5 The function of myristoylation of EV71 in membrane interaction. **A** Confocal microscopy images of VP4-WT-GFP and VP4-G2A-GFP protein distribution. Wild type (WT) VP4 and myristoylation-deficient (G2A) VP4 plasmids were transfected into 293T cells. After 24 h, the distribution of proteins in cells was observed by laser scanning confocal microscopy. The cell nuclei were stained with DAPI (blue) and VP4-WT-GFP or VP4-G2A-GFP is visualized in green. Scale bar = 20 μm. **B** Western blot analysis of VP4-G2A-GFP protein distribution compared to VP4-WT-GFP. Cytoplasmic fraction and membrane protein fraction were analyzed with Western blotting using an anti-GFP monoclonal antibody. GAPDH was used as an internal control for cytoplasmic protein. ATPA1 was used as an internal control for membrane protein (Zhu *et al.* 2017). Total is the total proteins from cells transfected with VP4-WT-GFP or VP4-G2A-GFP plasmids. **C** Percentage of VP4-GFP protein distribution in the cytoplasm or membrane based on grayscale measurement of Western blotting (**B**). Data presented as mean ± SD of three independent experiments. ***$P < 0.001$.

The Myristyl Groups Mediate Permeability in Model Membranes

In human rhinoviruses (HRV) and PV, the interaction of VP4 with membranes following its release from the particle suggests a potential role for VP4 in the membrane alterations required for genome transfer (Davis *et al.* 2008). Here, we described the EV71 VP4 as synthetic peptides, and investigated its ability to interact with, and induce, permeability in lipid membranes in the form of liposomes. Liposomes containing the carboxyfluorescein (CF) dye were allowed to interact with the WT or G2A VP4 proteins. Since CF becomes quenched at a high concentration, if myristic acid interacts with the liposome, CF will leak out of liposome, lowering its concentration and producing fluorescence. If myristic acid does not interact with the liposomes, CF concentration will remain high in the liposome and not be detected via immunofluorescence. We also performed the same experiment using the truncated VP4 peptide consisting of the initial 20 amino acids at the 5′ end of VP4 (VP4-20aa). VP4-20aa included the site of myristoylation, while eliminating the membrane interaction effect of the full VP4 protein (Fuchs and Blaas 2010; Zauner *et al.* 1995). HRV VP4 was included as a positive control (Zauner *et al.* 1995). At a concentration of 30 nmol/L, both WT and G2A VP4 induced the release of CF from liposomes. However, the rate of CF release in WT VP4 was faster than that for G2A VP4 (Fig. 6A). After 30 min, the luciferase activity of WT VP4 was distinctly higher than that induced by G2A VP4 (Fig. 6B). However, the rate of CF release from liposomes was not significantly different between VP4-20aa and the full-length VP4, while the rate of CF release induced by unmyristoylated peptides (VP4-G2A-20aa) was slower (Fig. 6C). Finally, the luciferase activity of VP4-WT-20aa was distinctly higher than that induced by the VP4-G2A-20aa (Fig. 6D). From these results, we concluded that both VP4 peptides and short peptides containing 20 amino acids can interact with liposomes so long as they can undergo myristoylation. Hence, myristic acid appears to mediate the viral interaction with the host cell membrane, while myristoylation enhances cell permeability.

Discussion

Many viruses contain N-terminal modifications to their viral proteins that include glycine linkages with myristic acid, which is a process known as myristoylation. Subsequently, there is a large amount of research on host-dependent viral protein lipid modification. Myristoylation is ubiquitous in viruses and cells and studies have

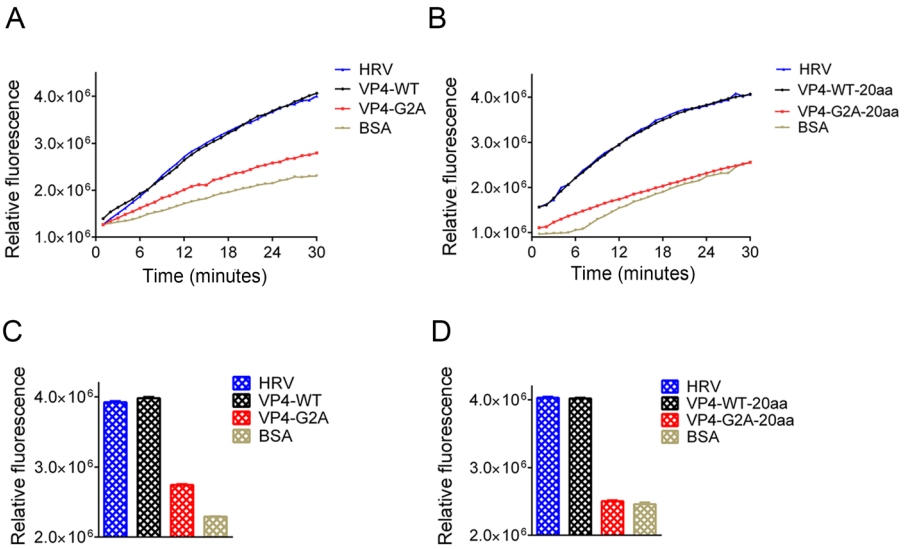

Fig. 6 Effect of myristoylation on membrane permeability measured by the release and fluorescent dequenching of carboxyfluorescein (CF) from liposomes. **A** Luciferase activity was detected after time course of CF dye release induced by 30 nmol/L myristoylated (VP4-WT), unmyristoylated (VP4-G2A) VP4, or BSA alone. The release induced by 30 nmol/L HRV VP4 (HRV) was shown as a positive control. The data shown are representatives of multiple experiments. **B** Relative rates of CF release for myristoylated VP4 (VP4-WT), unmyristoylated VP4 (VP4-G2A), and BSA alone. Data were calculated by fitting a straight line to the last four data points of the time course. **C** Luciferase activity was detected after time course of CF release induced by 30 nmol/L myristoylated (VP4-WT-20aa) or unmyristoylated (VP4-G2A-20aa) and BSA alone. The data shown are representative of multiple experiments. **D** Relative rates of CF release for the first 20 amino acid peptides of myristoylated VP4 (VP4-WT-20aa), unmyristoylated VP4 (VP4-G2A-20aa), and BSA alone, and positive control HRV VP4 (HRV) were calculated by fitting a straight line to the last four data points of the time course. Data are presented as mean ± SD of three independent experiments.

increasingly focused on identifying proteins with new lipid modifications to understand the role of myristoylation in the biological functions of these proteins.

Poliovirus and other members of the picornavirus family were the first non-enveloped viruses identified to contain myristoyl modification on their VP4 capsid protein (Chow *et al.* 1987). Mutation of the myristoyl site in poliovirus is the main way to study the function of myristoylation. Myristoylation is degraded or completely deleted by substituting a different amino acid residue in the myristoylation consensus sequence (6–8 amino acid residues at the N-terminus of the VP4 protein). In poliovirus, the second glycine at the N-terminus of VP4 was mutated to alanine (Gly-to-Ala) so that VP0 could not be myristoylated, but the replication of mutant RNA was not affected (Krausslich *et al.* 1990). This indicates that the Gly-to-Ala mutation alone does not affect the function of the viral protein even though myristoylation is impaired. Therefore, in our study, we also performed a Gly-to-Ala mutation on EV71 VP4 to obtain a myristoylation-deficient virus.

Although the myristoylation site has been completely determined, its exact role in the assembly process of the picornavirus is unclear. Moscufo *et al.* studied the assembly process of the VP4003A.D mutant poliovirus and revealed that its myristoylation level was down-regulated by approximately 50% (Moscufo *et al.* 1991). Studies have shown that the process of unmyristoylated protomers forming pentamers is attenuated and the unmyristoylated empty capsids accumulate; however, in mature virus particles, the level of myristoylation of the proteins was normal (Krausslich *et al.* 1990). Therefore, myristoylated protomers are preferentially selected to regulate the kinetics of pentamer formation. Subsequently, during the final stages of viral assembly, including RNA encapsulation and conversion of provirus to mature virions, myristoylated proteins are required to participate in these processes (Moscufo *et al.* 1991). Experiments have also shown that, contrary to the above results, the processing of myristoylated and non-myristoylated proteins in the mutants is similar (Krausslich *et al.* 1990). In our study, we demonstrated that the loss of myristoylation did not affect protein expression or the appearance of EV71 virus particles. After transfecting the mutant plasmid into cells, viral proteins were detected in the mutant variant. The appearance of the mutant and WT viruses were indistinguishable by electron microscopy. As shown in Fig. 1.

Although protein production and virus appearance were not affected by the loss of myristoylation, we did observe reduced infectivity in the mutant virus. Poliovirus with the Gly-to-Ala mutation (G4002A) could not infect HeLa cells (Moscufo *et al.* 1991), and when five amino acids at the N-terminus of poliovirus were mutated, the first (Gly-to-Arg), second (Ala-to-Pro) and fifth (Ser-to-Pro) position mutations prevented myristoylation of the protein precursor P1 and were lethal to the virus (Marc *et al.* 1989). These findings are consistent with the conclusions in our study, which showed that in pseudoviruses, the loss of myristoylation led to a decrease in viral infectivity (Fig. 2A, 2B). In myristoylation-deficient virus system, we found that CPE could not be produced after the myristoylation-deficient virus had infected cells (Fig. 2C). Viral proteins were also not detected in infected cells (Fig. 2D). Through the process of cell blind passaging, viruses were accumulated and detected in infected cells via immunofluorescence assaying (Fig. 2G), however, viral RNA replication was low (Fig. 2F). Furthermore, we compared the growth curve of G2A to WT (Fig. 3). It is suggested that loss of myristoylation blocked the viral RNA replication, which is consistent with the results reported in common cold virus (Mousnier *et al.* 2018). Negative-strand RNA was also measured after virus-infected host cells, we found that the negative RNA amount of WT virus increased over time, but the amount of myristoylation-deficient, virus infected the cells with inhibitor 2-HMA and NH_4Cl decreased significantly (Fig. 4). Myristoylation probably plays a vital role in the early stage of infection, but may not be involved in receptor binding. Myristyl groups were on the interior of the capsid. Surfaces of major picornavirus have a corrugated topography found at the five-fold axis of symmetry, surrounded by a deep depression (canyon) and another protrusion at the threefold axis. The canyons of enteroviruses are the sites of interaction with cell receptors (Chapman and Rossmann 1993). As shown in Fig. 1, as long as there was viral RNA as a template for viral replication, the process of RNA replication, viral proteins expression, and viral assembly could operate normally in the G2A mutant. During the replication of EV71 viral RNA, the virus needs to synthesize negative-strand RNA using virus mRNA as a template (Paul *et al.* 2000). According to the results, we conclude that there was no viral RNA releasing into the cells infected with myristoylation-deficient viruses.

There are many N-myristoyl-modified proteins that bind to the membrane (Courtneidge and Bishop 1982; Heuckeroth and Gordon 1989; Johnson *et al.* 1990; Rein *et al.* 1986; Rhee and Hunter 1987), and we asked if the distribution of VP4 proteins was associated with its myristoylated or unmyristoylated status after host cell infection. We found that in the cells transfected with myristoylation-deficient VP4, the localization of viral proteins changed from typical aggregation points at the membrane to a more dispersed pattern of localization in the cytoplasm (Fig. 5A). A plasma membrane separation experiment that indicated myristoylation of EV71 does affect virus interaction with the hose cell membrane structure (Fig. 5B, 5C). We found that myristyl groups could interact with the host membrane structure. To more

directly illustrate the role of myristoylation of EV71 interactions with membrane structure, we performed a liposome leakage assay. From these results, we found that the myristoylated VP4 protein interacted with the endocytic vesicle-like structure to release CF in it, and the myristoylation-deficient VP4 protein attenuated this effect (Fig. 6A, 6B). After disrupting the integrity of the VP4 protein, the loss of myristoylation significantly diminished the interaction of the VP4 protein with the host cell membrane structure (Fig. 6C, 6D). In enteroviruses, the capsid undergoes a conformational change that allows the viral RNA to be transferred across the plasma membrane and/or endosomal membrane into the cytoplasm through a yet completely defined mechanism (Strauss *et al.* 2013), and myristoyl group could affect viral RNA release. From these concludes, we speculate that during virus uncoating, myristoyl group interacts with endosomal membrane and disrupts the membrane, allowing viral RNA to be released into the cytoplasm. However, VP4 is only one capsid protein unit of EV71 and does not represent the natural condition of viral infection. Further exploration is needed to understand its mechanism.

Based on the above experimental results, we hypothesize that during the EV71 infection process, especially uncoating, VP4 extends from the interior of the five-fold axis and myristic acid covalently linked to the N-terminus of VP4 that interacts with the membrane of endocytic vesicle, resulting in the broken of the endocytic vesicle. A channel is then formed, and the viral genome leaves the capsid through the channel to enter the host cell.

This work is important to the research field in developing a fundamental understanding of enteroviruses and their life cycles. It also potentially has implications in clinical research or treatment of viral infection.

Acknowledgements This study was supported by the National Natural Science Foundation of China (Grant No. 31770184).

Author Contributions WS, and CJ concepted and supervised the study. JC and MQ performed the experiments. HL, XW, and FL assisted to perform part of the experiments. MQ, AH, YZ, BS, LC, SW and CJ helped to analyze the data. JC, WS and CJ drafted and edited the manuscript. All authors read and approved the final manuscript.

Compliance with Ethical Standards

Conflict of interest The authors declare that they have no conflict of interest.

Animal and Human Rights Statement This article does not contain any studies with human or animal subjects performed by any of the authors.

References

Alexander JP Jr, Baden L, Pallansch MA, Anderson LJ (1994) Enterovirus 71 infections and neurologic disease—United States, 1977–1991. J Infect Dis 169:905–908

Ansardi DC, Porter DC, Morrow CD (1992) Myristylation of poliovirus capsid precursor P1 is required for assembly of subviral particles. J Virol 66:4556–4563

Arita M, Nagata N, Sata T, Miyamura T, Shimizu H (2006) Quantitative analysis of poliomyelitis-like paralysis in mice induced by a poliovirus replicon. J Gen Virol 87:3317–3327

Boutin JA (1997) Myristoylation. Cell Signal 9:15–35

Braam B, Verhaar MC (2007) Understanding eNOS for pharmacological modulation of endothelial function: a translational view. Curr Pharm Des 13:1727–1740

Bryant M, Ratner L (1990) Myristoylation-dependent replication and assembly of human immunodeficiency virus 1. Proc Natl Acad Sci USA 87:523–527

Cao J, Liu H, Qu M, Hou A, Zhou Y, Sun B, Cai L, Gao F, Su W, Jiang C (2019) Determination of the cleavage site of enterovirus 71 VP0 and the effect of this cleavage on viral infectivity and assembly. Microb Pathog 134:103568

Chapman MS, Rossmann MG (1993) Comparison of surface properties of picornaviruses: strategies for hiding the receptor site from immune surveillance. Virology 195:745–756

Chow M, Moscufo N (1995) Myristoyl modification of viral proteins: assays to assess functional roles. Methods Enzymol 250:495–509

Chow M, Newman JF, Filman D, Hogle JM, Rowlands DJ, Brown F (1987) Myristylation of picornavirus capsid protein VP4 and its structural significance. Nature 327:482–486

Chumakov M, Voroshilova M, Shindarov L, Lavrova I, Gracheva L, Koroleva G, Vasilenko S, Brodvarova I, Nikolova M, Gyurova S, Gacheva M et al (1979) Enterovirus 71 isolated from cases of epidemic poliomyelitis-like disease in Bulgaria. Arch Virol 60:329–340

Colomer-Lluch M, Serra-Moreno R (2017) BCA2/Rabring7 Interferes with HIV-1 proviral transcription by enhancing the SUMOylation of IκBα. J Virol 91:e02098-16

Corbic Ramljak I, Stanger J, Real-Hohn A, Dreier D, Wimmer L, Redlberger-Fritz M, Fischl W, Klingel K, Mihovilovic MD, Blaas D, Kowalski H (2018) Cellular N-myristoyltransferases play a crucial picornavirus genus-specific role in viral assembly, virion maturation, and infectivity. PLoS Pathog 14:e1007203

Courtneidge SA, Bishop JM (1982) Transit of pp60v-src to the plasma membrane. Proc Natl Acad Sci USA 79:7117–7121

Davis MP, Bottley G, Beales LP, Killington RA, Rowlands DJ, Tuthill TJ (2008) Recombinant VP4 of human rhinovirus induces permeability in model membranes. J Virol 82:4169–4174

Eash S, Querbes W, Atwood WJ (2004) Infection of vero cells by BK virus is dependent on caveolae. J Virol 78:11583–11590

Farazi TA, Waksman G, Gordon JI (2001) The biology and enzymology of protein N-myristoylation. J Biol Chem 276:39501–39504

Filman DJ, Syed R, Chow M, Macadam AJ, Minor PD, Hogle JM (1989) Structural factors that control conformational transitions and serotype specificity in type 3 poliovirus. EMBO J 8:1567–1579

Fuchs R, Blaas D (2010) Uncoating of human rhinoviruses. Rev Med Virol 20:281–297

Geyer M, Peterlin BM (2001) Domain assembly, surface accessibility and sequence conservation in full length HIV-1 Nef. FEBS Lett 496:91–95

Giese SI, Woerz I, Homann S, Tibroni N, Geyer M, Fackler OT (2006) Specific and distinct determinants mediate membrane

binding and lipid raft incorporation of HIV-1(SF2). Nef Virol 355:175–191
Goodwin S, Tuthill TJ, Arias A, Killington RA, Rowlands DJ (2009) Foot-and-mouth disease virus assembly: processing of recombinant capsid precursor by exogenous protease induces self-assembly of pentamers *in vitro* in a myristoylation-dependent manner. J Virol 83:11275–11282
Gordon JI, Duronio RJ, Rudnick DA, Adams SP, Gokel GW (1991) Protein N-myristoylation. J Biol Chem 266:8647–8650
Heuckeroth RO, Gordon JI (1989) Altered membrane association of p60v-src and a murine 63-kDa N-myristoyl protein after incorporation of an oxygen-substituted analog of myristic acid. Proc Natl Acad Sci USA 86:5262–5266
Hill BT, Skowronski J (2005) Human N-myristoyltransferases form stable complexes with lentiviral nef and other viral and cellular substrate proteins. J Virol 79:1133–1141
Horodniceanu F, Panon G, Le Fur R, Barme M (1979) Purification of poliovirus obtained from human diploid cells by means of DEAE-Sepharose. Dev Biol Stand 42:75–80
Jiang P, Liu Y, Ma HC, Paul AV, Wimmer E (2014) Picornavirus morphogenesis. Microbiol Mol Biol Rev 78:418–437
Jin J, Xu L, Guo SJ, Sun SY, Zhang S, Zhu CL, Kong W, Jiang CL (2012) Safe and objective assay of enterovirus 71 neutralizing antibodies via pseudovirus. Chem Res Chin U 28:91–95
Jin J, Ma H, Xu L, An D, Sun S, Huang X, Kong W, Jiang C (2013) Development of a Coxsackievirus A16 neutralization assay based on pseudoviruses for measurement of neutralizing antibody titer in human serum. J Virol Methods 187:362–367
Johnson DR, Cox AD, Solski PA, Devadas B, Adams SP, Leimgruber RM, Heuckeroth RO, Buss JE, Gordon JI (1990) Functional analysis of protein N-myristoylation: metabolic labeling studies using three oxygen-substituted analogs of myristic acid and cultured mammalian cells provide evidence for protein-sequence-specific incorporation and analog-specific redistribution. Proc Natl Acad Sci USA 87:8511–8515
Johnson DR, Bhatnagar RS, Knoll LJ, Gordon JI (1994) Genetic and biochemical studies of protein N-myristoylation. Annu Rev Biochem 63:869–914
Krausslich HG, Holscher C, Reuer Q, Harber J, Wimmer E (1990) Myristoylation of the poliovirus polyprotein is required for proteolytic processing of the capsid and for viral infectivity. J Virol 64:2433–2436
Lee YM, Chow M (1992) Myristate modification does not function as a membrane association signal during poliovirus capsid assembly. Virology 187:814–820. https://doi.org/10.1016/0042-6822(92)90485-8
Li X, Fan P, Jin J, Su W, An D, Xu L, Sun S, Zhang Y, Meng X, Gao F, Kong W, Jiang C (2013) Establishment of cell lines with increased susceptibility to EV71/CA16 by stable overexpression of SCARB2. Virol J 10:250
Lin YW, Lin HY, Tsou YL, Chitra E, Hsiao KN, Shao HY, Liu CC, Sia C, Chong P, Chow YH (2012) Human SCARB2-mediated entry and endocytosis of EV71. PLoS ONE 7:e30507
Lum LC, Wong KT, Lam SK, Chua KB, Goh AY (1998) Neurogenic pulmonary oedema and enterovirus 71 encephalomyelitis. Lancet 352:1391
Marc D, Drugeon G, Haenni AL, Girard M, van der Werf S (1989) Role of myristoylation of poliovirus capsid protein VP4 as determined by site-directed mutagenesis of its N-terminal sequence. EMBO J 8:2661–2668
Marc D, Masson G, Girard M, van der Werf S (1990) Lack of myristoylation of poliovirus capsid polypeptide VP0 prevents the formation of virions or results in the assembly of noninfectious virus particles. J Virol 64:4099–4107
Mariani R, Skowronski J (1993) CD4 down-regulation by nef alleles isolated from human immunodeficiency virus type 1-infected individuals. Proc Natl Acad Sci USA 90:5549–5553
Martin-Belmonte F, Lopez-Guerrero JA, Carrasco L, Alonso MA (2000) The amino-terminal nine amino acid sequence of poliovirus capsid VP4 protein is sufficient to confer N-myristoylation and targeting to detergent-insoluble membranes. Biochemistry 39:1083–1090
Martinez A, Traverso JA, Valot B, Ferro M, Espagne C, Ephritikhine G, Zivy M, Giglione C, Meinnel Tl (2008) Extent of N-terminal modifications in cytosolic proteins from eukaryotes. Proteomics 8:2809–2831
Maurer-Stroh S, Eisenhaber B, Eisenhaber F (2002) N-terminal N-myristoylation of proteins: prediction of substrate proteins from amino acid sequence. J Mol Biol 317:541–557
Moscufo N, Simons J, Chow M (1991) Myristoylation is important at multiple stages in poliovirus assembly. J Virol 65:2372–2380
Mousnier A, Bell AS, Swieboda DP, Morales-Sanfrutos J, Perez-Dorado I, Brannigan JA, Newman J, Ritzefeld M, Hutton JA, Guedan A, Asfor AS, Robinson SW, Hopkins-Navratilova I, Wilkinson AJ, Johnston SL, Leatherbarrow RJ, Tuthill TJ, Solari R, Tate EW (2018) Fragment-derived inhibitors of human N-myristoyltransferase block capsid assembly and replication of the common cold virus. Nat Chem 10:599–606
Olokoltsov AA, Deniger D, Fleming EH, Roberts NJ Jr, Karpilow JM, Davey RA (2007) Small interfering RNA profiling reveals key role of clathrin-mediated endocytosis and early endosome formation for infection by respiratory syncytial virus. J Virol 81:7786–7800
Paul AV, Schultz A, Pincus SE, Oroszlan S, Wimmer E (1987) Capsid protein VP4 of poliovirus is N-myristoylated. Proc Natl Acad Sci USA 84:7827–7831
Paul AV, Rieder E, Kim DW, van Boom JH, Wimmer E (2000) Identification of an RNA hairpin in poliovirus RNA that serves as the primary template in the *in vitro* uridylylation of VPg. J Virol 74:10359–10370
Peng B, Robert-Guroff M (2001) Deletion of N-terminal myristoylation site of HIV Nef abrogates both MHC-1 and CD4 down-regulation. Immunol Lett 78:195–200
Raju RV, Magnuson BA, Sharma RK (1995) Mammalian myristoyl CoA: protein N-myristoyltransferase. Mol Cell Biochem 149–150:191–202
Rein A, McClure MR, Rice NR, Luftig RB, Schultz AM (1986) Myristylation site in Pr65gag is essential for virus particle formation by Moloney murine leukemia virus. Proc Natl Acad Sci USA 83:7246–7250. https://doi.org/10.1073/pnas.83.19.7246
Resh MD (1999) Fatty acylation of proteins: new insights into membrane targeting of myristoylated and palmitoylated proteins. Biochim Biophys Acta 1451:1–16
Rhee SS, Hunter E (1987) Myristylation is required for intracellular transport but not for assembly of D-type retrovirus capsids. J Virol 61:1045–1053
Strauss M, Levy HC, Bostina M, Filman DJ, Hogle JM (2013) RNA transfer from poliovirus 135S particles across membranes is mediated by long umbilical connectors. J Virol 87:3903–3914
Strecker T, Maisa A, Daffis S, Eichler R, Lenz O, Garten W (2006) The role of myristoylation in the membrane association of the Lassa virus matrix protein Z. Virol J 3:93
Tan YW, Hong WJ, Chu JJ (2016) Inhibition of enterovirus VP4 myristoylation is a potential antiviral strategy for hand, foot and mouth disease. Antiviral Res 133:191–195
Thinon E, Serwa RA, Broncel M, Brannigan JA, Brassat U, Wright MH, Heal WP, Wilkinson AJ, Mann DJ, Tate EW (2014) Global profiling of co- and post-translationally N-myristoylated proteomes in human cells. Nat Commun 5:4919

Udenwobele DI, Su RC, Good SV, Ball TB, Varma Shrivastav S, Shrivastav A (2017) Myristoylation: an important protein modification in the immune response. Front Immunol 8:751

Wagner E, Plank C, Zatloukal K, Cotten M, Birnstiel ML (1992) Influenza virus hemagglutinin HA-2 N-terminal fusogenic peptides augment gene transfer by transferrin-polylysine-DNA complexes: toward a synthetic virus-like gene-transfer vehicle. Proc Natl Acad Sci USA 89:7934–7938

Weaver TA, Panganiban AT (1990) N myristoylation of the spleen necrosis virus matrix protein is required for correct association of the Gag polyprotein with intracellular membranes and for particle formation. J Virol 64:3995–4001

Wilcox C, Hu JS, Olson EN (1987) Acylation of proteins with myristic acid occurs cotranslationally. Science 238:1275–1278

Wills JW, Craven RC, Achacoso JA (1989) Creation and expression of myristylated forms of Rous sarcoma virus gag protein in mammalian cells. J Virol 63:4331–4343

Wright MH, Heal WP, Mann DJ, Tate EW (2010) Protein myristoylation in health and disease. J Chem Biol 3:19–35

Xu L, Su W, Jin J, Chen J, Li X, Zhang X, Sun M, Sun S, Fan P, An D, Zhang H, Zhang X, Kong W, Ma T, Jiang C (2014) Identification of luteolin as enterovirus 71 and coxsackievirus A16 inhibitors through reporter viruses and cell viability-based screening. Viruses 6:2778–2795

Zauner W, Blaas D, Kuechler E, Wagner E (1995) Rhinovirus-mediated endosomal release of transfection complexes. J Virol 69:1085–1092

Zhang J, Dong M, Jiang B, Dai X, Meng J (2012) Antigenic characteristics of the complete and truncated capsid protein VP1 of enterovirus 71. Virus Res 167:337–342

Zhang YX, Huang YM, Li QJ, Li XY, Zhou YD, Guo F, Zhou JM, Cen S (2017) A highly conserved amino acid in VP1 regulates maturation of enterovirus 71. PLoS Pathog 13:e1006625

Zhu Y, Luo S, Sabo Y, Wang C, Tong L, Goff SP (2017) Heme oxygenase 2 binds myristate to regulate retrovirus assembly and TLR4 signaling. Cell Host Microbe 21:220–230